Iranian Journal of Numerical Analysis and Optimization
Vol. 15, No. 2, 2025, pp 704–727
https://doi.org/10.22067/ijnao.2025.91265.1571
https://ijnao.um.ac.ir/

Research Article

Numerical design of nonstationary wavelets: Enhanced filter design ...

A. Boussaad, Y. Fourar* and K. Melkemi

Abstract

In this study, we propose a novel method for computing both primal and dual filters for nonstationary biorthogonal wavelets, offering an advanced approach to wavelet filter design. The key challenge in image compression that this study addresses is the inefficiency of conventional stationary wavelets, which rely on fixed filter banks that do not adapt to local variations in an image. This limitation results in suboptimal compression performance, particularly for images with varying statistical properties and localized features. To address this, we use a nonstationary biorthogonal filter banks, which modify basis functions at different scaling levels, leading

*Corresponding author

Received 22 December 2024; revised 20 February 2025; accepted 2 March 2025

Abdelmalik Boussaad
Department of Mathematics, Faculty of Mathematics And Computer Science, University of Batna 2, Algeria. e-mail: a.boussaad2001@gmail.com

Yasmine Fourar
Department of Mathematics, Faculty of Mathematics And Computer Science, University of Batna 2, Algeria. e-mail: ya.fourar@univ-batna2.dz

Khaled Melkemi
Department of Mathematics, Faculty of Mathematics And Computer Science, University of Batna 2, Algeria. e-mail: k.melkemi@univ-batna2.dz

How to cite this article
Boussaad, A. Fourar, Y. and Melkemi, K., Numerical design of nonstationary wavelets: Enhanced filter design andapplications in image compression. *Iran. J. Numer. Anal. Optim.*, 2025; 15(2): 704-727. https://doi.org/10.22067/ijnao.2025.91265.1571

to improved frequency resolution, signal representation, and compression efficiency.

Our technique employs cardinal Chebyshev B-splines to derive explicit formulas for the primal filters, enabling precise calculation of filter coefficients essential for wavelet transforms. Additionally, we enforce normality and biorthogonality conditions within nonstationary multiresolution analysis to maintain the relationship between primal and dual wavelet filters at each scaling level. This structured approach allows for explicit formulation of the dual filters while ensuring accurate decomposition and reconstruction. Experimental results confirm that the proposed method improves compression efficiency over conventional Daubechies biorthogonal filters, increasing the number of zero coefficients in compressed images. This leads to better visual quality and reduced storage requirements while maintaining computational efficiency. Such improvements are particularly beneficial in applications requiring high-fidelity image reconstruction, such as medical imaging, satellite data processing, and video compression. MATLAB simulations validate the effectiveness of the approach, making it a promising alternative for image processing and data compression applications.

AMS subject classifications (2020): Primary 42C40; Secondary 65T60, 42C10.

Keywords: Cardinal Chebyshev B-splines; Biorthogonality; Wavelets; Image compression.

1 Introduction

Biorthogonal wavelets form a distinct class of wavelets that, unlike orthogonal wavelets [6, 4], employ separate functions for analysis and reconstruction. This fundamental distinction allows for greater flexibility in signal representation and improved frequency resolution, making them particularly useful in various signal processing applications. Key properties of biorthogonal wavelets include:

- **Symmetry**: They can be designed with varying degrees of symmetry, which is beneficial for specific applications.

- **Smoothness**: Greater smoothness corresponds to more vanishing moments, enabling better approximations of signals with smooth variations.

- **Compact Support**: Their scaling and wavelet functions are nonzero only over a finite interval, ensuring computational efficiency in fast algorithms like the discrete wavelet transform.

Nonstationary biorthogonal wavelets extend these advantages by adaptively adjusting their basis functions at each scaling level, based on the signal's properties. This adaptability enhances their ability to represent localized features or varying statistical properties, making them particularly effective in image processing, audio signal processing, and biomedical signal analysis. In contrast, stationary biorthogonal wavelets rely on a fixed set of basis functions, which may not be optimal for signals with complex characteristics.

A key advancement in this field is the use of *cardinal Chebyshev B-splines* [8, 7, 2] as a basis for constructing nonstationary biorthogonal wavelets. These splines offer excellent time-frequency localization properties, making them highly effective for analyzing nonstationary signals. Previous studies have explored their applications in wavelet construction. For example, Lee and Yoon [5] introduced a lifting scheme-based algorithm that enhances wavelet approximation properties and computational efficiency. Similarly, Vonesch, Blu, and Unser [10] developed a family of generalized Daubechies wavelets [3] incorporating Chebyshev B-splines, and Boxing. Zhang et al. [11] proposed a construction method based on exponential pseudo-splines.

While significant progress has been made, current methods for designing nonstationary biorthogonal wavelets still face several challenges, particularly in computational efficiency and systematic filter design. Many approaches rely on iterative or heuristic techniques, which can be computationally intensive and lack a structured framework. Additionally, solving the underlying systems of equations during wavelet construction remains a computational bottleneck, limiting practical applications in real-time or resource-constrained environments.

To address these challenges, this paper introduces a novel approach that systematically derives a linear system based on the normality and biorthogonality conditions of nonstationary multiresolution analysis. Our key contributions include:

- **Novel Design Method**: We propose a new method for constructing nonstationary biorthogonal wavelets using fundamental conditions from multiresolution analysis [9].
- **Efficient Numerical Solution**: By formulating a linear system, we enable the use of direct numerical methods such as Gauss–Jordan elimination and LU factorization, improving computational efficiency.
- **Explicit Filter Formulation**: Our approach provides explicit formulas for filters and dual filters at all scaling levels, ensuring a systematic and practical wavelet design process.
- **Comprehensive Framework**: We integrate theoretical insights with practical applications, making our method accessible to both researchers and practitioners in signal processing.

The remainder of this paper is structured as follows: Section 2 provides an overview of nonstationary biorthogonal multiresolution analysis, including key definitions and properties. Section 3 explores the use of cardinal Chebyshev B-splines in constructing nonstationary biorthogonal wavelets. By the conclusion, readers will gain a comprehensive understanding of the theory, practical applications, and our novel design method for nonstationary biorthogonal wavelets.

2 Definitions and properties of biorthogonal nonstationary wavelets

Let $(\mathcal{V}_j)_{j\leq j_0}$ and $(\widetilde{\mathcal{V}}_j)_{j\leq j_0}$ be a pair of **NSRMAs** [1] generated by a pair of dual scaling functions φ_j and $\widetilde{\varphi}_j$, $j \leq j_0$, such that

$$\langle \varphi_j, \widetilde{\varphi}_j(. - k)\rangle = \delta_{0,k}, \qquad k \in \mathbb{Z}. \tag{1}$$

The concept of biorthogonal wavelets is to find complementary spaces $\mathcal{W}_j$ and $\widetilde{\mathcal{W}}_j$ satisfying

$$\mathcal{V}_{j+1} = \mathcal{V}_j + \mathcal{W}_j, \text{ and } \widetilde{\mathcal{V}}_{j+1} = \widetilde{\mathcal{V}}_j + \widetilde{\mathcal{W}}_j, \tag{2}$$

$$\mathcal{W}_j \perp \widetilde{\mathcal{V}}_j, \text{ and } \widetilde{\mathcal{W}}_j \perp \mathcal{V}_j. \tag{3}$$

The nesting property for the subspaces $\mathcal{V}_j$ and $\widetilde{\mathcal{V}}_j$, implies the existence of filters $h_j = (h_j[k])_{k\in\mathbb{Z}} \in \ell^2(\mathbb{Z})$, $\widetilde{h}_j = (\widetilde{h}_j[k])_{k\in\mathbb{Z}} \in \ell^2(\mathbb{Z})$, $j \le j_0$, which satisfy

$$\varphi_j(t) = \sqrt{2}\sum_{k\in\mathbb{Z}} h_j[k]\varphi_{j+1}(2t-k), \quad \widetilde{\varphi}_j(t) = \sqrt{2}\sum_{k\in\mathbb{Z}} \widetilde{h}_j[k]\widetilde{\varphi}_{j+1}(2t-k). \tag{4}$$

By the Fourier transform, we have

$$\widehat{\varphi}_j(\omega) = \mathcal{H}_j(e^{i\frac{\omega}{2}})\widehat{\varphi}_{j+1}\left(\frac{\omega}{2}\right), \tag{5}$$

$$\widehat{\widetilde{\varphi}}_j(\omega) = \widetilde{\mathcal{H}}_j(e^{i\frac{\omega}{2}})\widehat{\widetilde{\varphi}}_{j+1}\left(\frac{\omega}{2}\right), \tag{6}$$

with

$$\mathcal{H}_j(e^{i\omega}) = \frac{1}{\sqrt{2}}\sum_{k\in\mathbb{Z}} h_j[k]e^{-ik\omega}, \tag{7}$$

$$\widetilde{\mathcal{H}}_j(e^{i\omega}) = \frac{1}{\sqrt{2}}\sum_{k\in\mathbb{Z}} \widetilde{h}_j[k]e^{-ik\omega}. \tag{8}$$

We assume that $z = e^{-i\omega}$.

Proposition 1. The filters $\mathcal{H}_j$ and $\widetilde{\mathcal{H}}_j$ associated for φ_j and $\widetilde{\varphi}_j$ satisfy the scaling condition:

$$\mathcal{H}_j(z)\widetilde{\mathcal{H}}_j(z^{-1}) + \mathcal{H}_j(-z)\widetilde{\mathcal{H}}_j(-z^{-1}) = 1. \tag{9}$$

For all $k \in \mathbb{Z}$, the preceding condition is equivalent to

$$\sum_{\ell\in\mathbb{Z}} \widetilde{h}_j[\ell]h_j[\ell-2k] = \delta_{k,0}. \tag{10}$$

Definition 1. The biorthogonal wavelet functions are given as follows:

$$\psi_j(t) = \sqrt{2}\sum_{k\in\mathbb{Z}} g_j[k]\varphi_{j+1}(2t-k), \quad \widetilde{\psi}_j(t) = \sqrt{2}\sum_{k\in\mathbb{Z}} \widetilde{g}_j[k]\widetilde{\varphi}_{j+1}(2t-k), \tag{11}$$

such that

$$\widetilde{g}_j[k] = (-1)^k h_j[1-k], \qquad g_j[k] = (-1)^k \widetilde{h}_j[1-k], \tag{12}$$

where

$$g_j = (g_j[k])_{k\in\mathbb{Z}}, \qquad \widetilde{g}_j = (\widetilde{g}_j[k])_{k\in\mathbb{Z}}, \tag{13}$$

are the scaling filters associated for ψ_j and $\widetilde{\psi}_j$, respectively.

For all $k \in \mathbb{Z}$, we have

$$\sum_{k\in\mathbb{Z}} h_j[k] = \sqrt{2}, \quad \sum_{k\in\mathbb{Z}} \widetilde{h}_j[k] = \sqrt{2}, \tag{14}$$

$$\sum_{k\in\mathbb{Z}} g_j[k] = 0, \quad \sum_{k\in\mathbb{Z}} \widetilde{g}_j[k] = 0. \tag{15}$$

As in the stationary case for a function $f \in L^2(\mathbb{R})$, a wavelet decomposition at level j_0 can be introduced, as follows:

$$f = \sum_{k\in\mathbb{Z}} a_{j_0}[k]\varphi_{j_0,k} + \sum_{j\le j_0}\sum_{k\in\mathbb{Z}} d_j[k]\psi_{j,k}, \tag{16}$$

where

$$a_{j_0}[k] = \langle f, \widetilde{\varphi}_{j_0,k}\rangle, \quad d_j[k] = \langle f, \widetilde{\psi}_{j,k}\rangle, \tag{17}$$

and

$$\widetilde{\varphi}_{j,k}(t) = 2^{j/2}\widetilde{\varphi}_j(2^j t - k), \qquad \widetilde{\psi}_{j,k}(t) = 2^{j/2}\widetilde{\psi}_j(2^j t - k). \tag{18}$$

3 Construction of scaling filters and dual scaling filters

The function we choose as a scaling function is the cardinal Chebyshev B-splines. Let us first recall the definition of the exponential Chebyshev B-splines mentioned in [1]. Let $\lambda = (\lambda_1, \ldots, \lambda_n)$ be a complex vector.

Definition 2. Suppose that $\alpha \in \mathbb{R}$. The function N_α^1 is defined by

$$N_\alpha^1(t) = e^{\alpha t}\chi_{[0,1]}(t), \qquad t \in \mathbb{R}. \tag{19}$$

Function N_λ^n is defined by convolution as follows:

$$N_{\lambda}^{n} = N_{\lambda_1}^{1} * \cdots * N_{\lambda_n}^{1}. \tag{20}$$

The function $N_{2^{-j}\lambda}^{n}(t)$ can generate a Riesz basis only if the vector λ does not have any distinct purely imaginary components λ_i and λ_j, where the difference between them equals $i2\pi k$ for some integer k.

For $n = 1$,

$$N_{\alpha}^{1}(t) = N_{\frac{\alpha}{2}}^{1}(2t) + e^{\frac{\alpha}{2}} N_{\frac{\alpha}{2}}^{1}(2t-1).$$

By the Fourier transform, we have

$$\widehat{N_{\alpha}^{1}}(\omega) = \left(\frac{1 + e^{\frac{\alpha - i\omega}{2}}}{2}\right) \widehat{N_{\frac{\alpha}{2}}^{1}}\left(\frac{\omega}{2}\right).$$

In the following, we assume that $\alpha \in [0, 10] \setminus \{2\pi\}$ with $2\pi \approx 6.2831$. This restriction ensures that the denominator remains nonzero for all the filters of the primal and dual functions.

3.1 Second order cardinal Chebyshev B-splines

Let $\lambda = (\lambda_1, \lambda_2) = (-i\alpha, i\alpha)$. We assume that

$$\varphi_j(t) = N_{2^{-j}\lambda}^{2}(t). \tag{21}$$

Then

$$\begin{aligned}
&\widehat{\varphi_j}(\omega) \\
&= \widehat{N_{2^{-j}\lambda_1}^{1}}(\omega) \widehat{N_{2^{-j}\lambda_2}^{1}}(\omega) \\
&= \frac{1}{4}\left(1 + (e^{2^{-(j+1)}\lambda_1} + e^{2^{-(j+1)}\lambda_2}) e^{\frac{-i\omega}{2}} + e^{2^{-(j+1)}(\lambda_1+\lambda_2)} e^{-i\omega}\right) \widehat{N_{2^{-(j+1)}\lambda}^{2}}\left(\frac{\omega}{2}\right) \\
&= \mathcal{H}_j\left(\frac{\omega}{2}\right) \widehat{\varphi_{j+1}}\left(\frac{\omega}{2}\right).
\end{aligned}$$

In accordance with (5), we obtain

$$h_j[0] = h_j[2] = \frac{\sqrt{2}}{4}, \qquad h_j[1] = \frac{2\sqrt{2}\cos(2^{-(j+1)}\alpha)}{4}.$$

However, these coefficients are not normalized. To normalize them, we simply divide by $\mathcal{H}_j(0)$, yielding

$$h_j[0] = h_j[2] = \frac{\sqrt{2}}{2 + 2\cos(2^{-(j+1)}\alpha)}, \qquad h_j[1] = \frac{2\sqrt{2}\cos(2^{-(j+1)}\alpha)}{2 + 2\cos(2^{-(j+1)}\alpha)}.$$

We will now introduce a method to explicitly determine the filters of dual scaling functions. Let the filters coefficients of the dual scaling functions $(\widetilde{\varphi}_j)_{j\le j_0}$ be $\widetilde{h}_j[-1]$, $\widetilde{h}_j[0]$, $\widetilde{h}_j[1]$, $\widetilde{h}_j[2]$, $\widetilde{h}_j[3]$. First, we assume that the dual scaling functions are symmetric, which means

$$\widetilde{h}_j[-1] = \widetilde{h}_j[3], \qquad \widetilde{h}_j[0] = \widetilde{h}_j[2].$$

The relation (14) implies

$$2\widetilde{h}_j[3] + 2\widetilde{h}_j[2] + \widetilde{h}_j[1] = \sqrt{2}. \tag{22}$$

Using (10) for $k = 0$, we obtain

$$\cos\left(2^{-(j+1)}\alpha\right)\widetilde{h}_j[1] + \widetilde{h}_j[2] = \frac{2 + 2\cos(2^{-(j+1)}\alpha)}{2\sqrt{2}}, \tag{23}$$

and for $k = 1$, we have

$$2\cos\left(2^{-(j+1)}\alpha\right)\widetilde{h}_j[3] + \widetilde{h}[2] = 0. \tag{24}$$

As an additional condition to simplify the calculation, we use (15) to get

$$\sum_{k=-2}^{2} (-1)^k \widetilde{h}_j[1-k] = 0,$$

which leads to

$$2\widetilde{h}_j[3] - 2\widetilde{h}_j[2] + \widetilde{h}_j[1] = 0. \tag{25}$$

To determine $\widetilde{h}_j[1]$, $\widetilde{h}_j[2]$, and $\widetilde{h}_j[3]$, the above system is solved using the Gaussian elimination.

Therefore,

$$\begin{cases} \widetilde{h}_j[-1] = \widetilde{h}_j[3] = -\dfrac{\sqrt{2}}{8\cos(2^{-(j+1)}\alpha)}, \\ \widetilde{h}_j[0] = \widetilde{h}_j[2] = \dfrac{\sqrt{2}}{4}, \\ \widetilde{h}_j[1] = \dfrac{2\sqrt{2}\cos(2^{-(j+1)}\alpha) + \sqrt{2}}{4\cos(2^{-(j+1)}\alpha)}. \end{cases}$$

3.2 Third order cardinal Chebyshev B-splines

Let $\lambda = (\lambda_1, \lambda_2, \lambda_3) = (0, -i\alpha, i\alpha)$, let $\widetilde{\lambda} = (\lambda_2, \lambda_3)$, and let

$$N^3_{\lambda}(x) = N^1_{\lambda_1} * N^2_{\widetilde{\lambda}}(x).$$

We assume that

$$\varphi_j(t) = N^3_{2^{-j}\lambda}(t). \tag{26}$$

Then

$$\begin{aligned} \widehat{\varphi_j}(\omega) &= \widehat{N^2_{2^{-j}\widetilde{\lambda}}}(\omega)\widehat{N^1_{2^{-j}\lambda_1}}(\omega), \\ &= \left(\frac{1}{8} + \frac{1+2\cos(2^{-(j+1)}\alpha)}{8}e^{-i\frac{\omega}{2}} + \frac{1+2\cos(2^{-(j+1)}\alpha)}{8}e^{-i\omega} + \frac{1}{8}e^{-i\frac{3\omega}{2}}\right) \\ &\quad \times \widehat{N^3_{2^{-(j+1)}\gamma}}\left(\frac{\omega}{2}\right) \\ &= \mathcal{H}_j\left(\frac{\omega}{2}\right)\widehat{\varphi_{j+1}}\left(\frac{\omega}{2}\right). \end{aligned}$$

The normalized coefficients are derived using the same method as described earlier:

$$\begin{aligned} h_j[0] = h_j[3] &= \frac{\sqrt{2}}{4 + 4\cos(2^{-(j+1)}\alpha)}, \\ h_j[1] = h_j[2] &= \frac{\sqrt{2}(2\cos(2^{-(j+1)}\alpha) + 1)}{4 + 4\cos(2^{-(j+1)}\alpha)}. \end{aligned}$$

Using the same steps as for $n = 2$, we assume that $\widetilde{h}_j[-1], \widetilde{h}_j[0], \widetilde{h}_j[1], \widetilde{h}_j[2]$, $\widetilde{h}_j[3]$, $\widetilde{h}_j[4]$, are the filters coefficients of the dual scaling functions$(\widetilde{\varphi}_j)_{j\leq j_0}$, subject to the condition that they are symmetric:

$$\widetilde{h}_j[-1] = \widetilde{h}_j[4], \qquad \widetilde{h}_j[0] = \widetilde{h}_j[3], \qquad \widetilde{h}_j[1] = \widetilde{h}_j[2].$$

The relation (14) implies

$$\widetilde{h}_j[2] + \widetilde{h}_j[3] + \widetilde{h}_j[4] = \frac{\sqrt{2}}{2}. \tag{27}$$

Using (10), we can find the following equations:

For $k = 0$,

$$(2\cos(2^{-(j+1)}\alpha) + 1)\widetilde{h}_j[2] + \widetilde{h}_j[3] = \frac{4 + 4\cos(2^{-(j+1)}\alpha)}{2\sqrt{2}}, \tag{28}$$

and for $k = 1$,

$$\widetilde{h}_j[2] + \left(2\cos(2^{-(j+1)}\alpha) + 1\right)\widetilde{h}_j[3] + \left(2\cos(2^{-(j+1)}\alpha) + 1\right)\widetilde{h}_j[4] = 0. \tag{29}$$

We can use Gaussian elimination to solve the above linear system and obtain $\widetilde{h}_j[2]$, $\widetilde{h}_j[3]$, and $\widetilde{h}_j[4]$, with the following explicit formulas:

$$\begin{cases} \widetilde{h}_j[-1] = \widetilde{h}_j[4] = 0, \\ \widetilde{h}_j[0] = \widetilde{h}_j[3] = \dfrac{-\sqrt{2}}{4\cos(2^{-(j+1)}\alpha)}, \\ \widetilde{h}_j[1] = \widetilde{h}_j[2] = \dfrac{2\sqrt{2}\cos(2^{-(j+1)}\alpha) + \sqrt{2}}{4\cos(2^{-(j+1)}\alpha)}. \end{cases}$$

3.3 Fourth order cardinal Chebyshev B-splines

Let $\lambda = (\delta_1, \delta_2)$, where $\delta_1 = (\lambda_1, \lambda_2) = (0, 0)$, $\delta_2 = (\lambda_3, \lambda_4) = (-i\alpha, i\alpha)$, and

$$N^4_\lambda(x) = N^2_{\delta_1} * N^2_{\delta_2}(x).$$

Then, we assume that

$$\varphi_j(t) = N^4_{2^{-j}\lambda}(t). \tag{30}$$

Then

$$\widehat{\varphi_j}(\omega) = \widehat{N^2_{2^{-j}\delta_1}}(\omega)\widehat{N^2_{2^{-j}\delta_2}}(\omega),$$

$$
\begin{aligned}
&= \left(\frac{1}{16} + \frac{2 + 2\cos(2^{-(j+1)}\alpha)}{16} e^{-i\frac{\omega}{2}} + \frac{2 + 4\cos(2^{-(j+1)}\alpha)}{16} e^{-i\omega} \right. \\
&\quad \left. + \frac{2 + 2\cos(2^{-(j+1)}\alpha)}{16} e^{-i\frac{3\omega}{2}} + \frac{1}{16} e^{2i\omega} \right) \widehat{N^4_{2^{-(j+1)}\lambda}} \left(\frac{\omega}{2} \right) \\
&= \mathcal{H}_j \left(\frac{\omega}{2} \right) \widehat{\varphi_{j+1}} \left(\frac{\omega}{2} \right),
\end{aligned}
$$

Following the same steps as before, we obtain the normalized coefficients:

$$
\begin{cases}
h_j[0] = h_j[4] = \dfrac{\sqrt{2}}{8 + 8(\cos(2^{-(j+1)}\alpha)}, \\
h_j[1] = h_j[3] = \dfrac{2\sqrt{2}(\cos(2^{-(j+1)}\alpha) + 1)}{8 + 8(\cos(2^{-(j+1)}\alpha)}, \\
h_j[2] = \dfrac{2\sqrt{2}(2\cos(2^{-(j+1)}\alpha) + 1)}{8 + 8(\cos(2^{-(j+1)}\alpha)}.
\end{cases}
$$

As before, let us assume that $\widetilde{h}_j[-1], \widetilde{h}_j[0], \widetilde{h}_j[1], \widetilde{h}_j[2], \widetilde{h}_j[3], \widetilde{h}_j[4], \widetilde{h}_j[5]$ are the filters coefficients of dual scaling functions. Moreover, to ensure that the dual scaling functions are symmetric, we set

$$
\widetilde{h}_j[-1] = \widetilde{h}_j[5], \quad \widetilde{h}_j[0] = \widetilde{h}_j[4], \quad \widetilde{h}_j[1] = \widetilde{h}_j[3].
$$

The relation (14) implies

$$
2\widetilde{h}_j[5] + 2\widetilde{h}_j[4] + 2\widetilde{h}_j[3] + \widetilde{h}_j[2] = \sqrt{2}. \tag{31}
$$

Using (10), we find, for $k = 0$,

$$
\begin{aligned}
&\widetilde{h}_j[4] + 2\left(\cos(2^{-(j+1)}\alpha) + 1\right)\widetilde{h}_j[3] + \left(2\cos(2^{-(j+1)}\alpha) + 1\right)\widetilde{h}_j[2] \\
&\qquad = \frac{8 + 8(\cos(2^{-(j+1)}\alpha)}{2\sqrt{2}},
\end{aligned} \tag{32}
$$

for $k = 1$,

$$
\begin{aligned}
&\widetilde{h}_j[2] + 2\left(\cos(2^{-(j+1)}\alpha) + 1\right)\widetilde{h}_j[3] + 2\left(2\cos(2^{-(j+1)}\alpha) + 1\right)\widetilde{h}_j[4] \\
&\qquad + 2\left(\cos(2^{-(j+1)}\alpha) + 1\right)\widetilde{h}_j[5] = 0,
\end{aligned} \tag{33}
$$

and for $k = 2$,

$$
\widetilde{h}[4] + 2\left(\cos(2^{-(j+1)}\alpha) + 1\right)\widetilde{h}_j[5] = 0. \tag{34}
$$

As in $n = 2$, we take the following additional condition to simplify the computation:

$$\sum_{k=-4}^{2} (-1)^k \widetilde{h}_j[1-k] = 0,$$

which implies

$$2\widetilde{h}_j[5] - 2\widetilde{h}_j[4] + 2\widetilde{h}_j[3] - \widetilde{h}_j[2] = 0. \tag{35}$$

Finally, we find $\widetilde{h}_j[2], \widetilde{h}_j[3], \widetilde{h}_j[4]$ and $\widetilde{h}_j[5]$ by the following formulas:

$$\begin{cases} \widetilde{h}_j[-1] = \widetilde{h}_j[5] = \dfrac{\sqrt{2}\cos(2^{-(j+1)}\alpha) + 2\sqrt{2}}{16\cos(2^{-(j+1)}\alpha) + 8\cos(2^{-j}\alpha) + 8}, \\ \widetilde{h}_j[0] = \widetilde{h}_j[4] = \dfrac{-6\sqrt{2}\cos(2^{-(j+1)}\alpha) - \sqrt{2}\cos(2^{-j}\alpha) - 5\sqrt{2}}{16\cos(2^{-(j+1)}\alpha) + 8\cos(2^{-j}\alpha) + 8}, \\ \widetilde{h}_j[1] = \widetilde{h}_j[3] \\ \qquad = \dfrac{8\sqrt{2}\cos(2^{-(j+1)}\alpha) + 7\sqrt{2}\cos(2^{-j}\alpha) + 2\sqrt{2}\cos(3\,2^{-(j+1)}\alpha) + 3\sqrt{2}}{56\cos(2^{-(j+1)}\alpha) + 32\cos(2^{-j}\alpha) + 8\cos(3\,2^{-(j+1)}\alpha) + 32}, \\ \widetilde{h}_j[2] = \dfrac{10\sqrt{2}\cos(2^{-(j+1)}\alpha) + 3\sqrt{2}\cos(2^{-j}\alpha) + 7\sqrt{2}}{8\cos(2^{-(j+1)}\alpha) + 4\cos(2^{-j}\alpha) + 4}. \end{cases}$$

3.4 Fifth order cardinal Chebyshev B-splines

Let $\lambda = (\delta_1, \delta_2)$, where $\delta_1 = (\lambda_1, \lambda_2, \lambda_3) = (0, 0, 0)$, $\delta_2 = (\lambda_4, \lambda_5) = (-i\alpha, i\alpha)$, and

$$N_\lambda^5(x) = N_{\delta_1}^3 * N_{\delta_2}^2(x).$$

Then we assume that

$$\varphi_j(t) = N_{2^{-j}\lambda}^5(t). \tag{36}$$

Therefore,

$$\begin{aligned} \widehat{\varphi_j}(\omega) &= \widehat{N_{2^{-j}\delta_1}^3}(\omega)\widehat{N_{2^{-j}\delta_2}^2}(\omega), \\ &= \frac{1}{32}\Big(1 + (1 + 4\cos(2^{-(j+1)}\alpha)e^{-i\frac{\omega}{2}} \end{aligned}$$

$$
\begin{aligned}
&+(4+4\cos(2^{-(j+1)}\alpha)+2\cos(2^{-j}\alpha))e^{-i\omega}\\
&+(4+4\cos(2^{-(j+1)}\alpha)+2\cos(2^{-j}\alpha))e^{-i\frac{3\omega}{2}}\\
&+(1+4\cos(2^{-(j+1)}\alpha)e^{-2i\omega}+e^{-i\frac{5\omega}{2}}\Big)\widehat{N^5_{2^{-j}\lambda}}\left(\frac{\omega}{2}\right)\\
&=\mathcal{H}_j\left(\frac{\omega}{2}\right)\widehat{\varphi_{j+1}}\left(\frac{\omega}{2}\right),
\end{aligned}
$$

So, the normalized coefficients are given by

$$
\begin{cases}
h_j[0]=h_j[5]=\dfrac{\sqrt{2}}{12+16\cos(2^{-(j+1)}\alpha)+4\cos(2^{-j}\alpha)},\\
h_j[1]=h_j[4]=\dfrac{\sqrt{2}(1+4\cos(2^{-(j+1)}\alpha)}{12+16\cos(2^{-(j+1)}\alpha)+4\cos(2^{-j}\alpha)},\\
h_j[2]=h_j[3]=\dfrac{2\sqrt{2}(2+2\cos(2^{-(j+1)}\alpha)+\cos(2^{-j}\alpha))}{12+16\cos(2^{-(j+1)}\alpha)+4\cos(2^{-j}\alpha)}.
\end{cases}
$$

We assume that $\widetilde{h}_j[-1],\widetilde{h}_j[0],\widetilde{h}_j[1],\widetilde{h}_j[2],\widetilde{h}_j[3],\widetilde{h}_j[4],\widetilde{h}_j[5]$, and $\widetilde{h}_j[6]$ are the filters coefficients of dual scaling functions. Moreover, to ensure that the dual scaling functions are symmetric, we put

$$
\widetilde{h}_j[-1]=\widetilde{h}_j[6],\quad \widetilde{h}_j[0]=\widetilde{h}_j[5],\quad \widetilde{h}_j[1]=\widetilde{h}_j[4],\quad \widetilde{h}_j[2]=\widetilde{h}_j[3].
$$

The relation (14) implies

$$
2\widetilde{h}_j[3]+2\widetilde{h}_j[4]+2\widetilde{h}_j[5]+2\widetilde{h}_j[6]=\sqrt{2}. \tag{37}
$$

Using (10), we find, for $k=0$,

$$
\begin{aligned}
&(4+4\cos(2^{-(j+1)}\alpha)+2\cos(2^{-j}\alpha))\widetilde{h}_j[3]+(1+4\cos(2^{-(j+1)}\alpha)\widetilde{h}_j[4]+\widetilde{h}_j[5]\\
&\qquad=\frac{12+16\cos(2^{-(j+1)}\alpha)+4\cos(2^{-j}\alpha)}{2\sqrt{2}},
\end{aligned} \tag{38}
$$

for $k=1$,

$$
\begin{aligned}
&(2+4\cos(2^{-(j+1)}\alpha)\widetilde{h}_j[3]+(4+4\cos(2^{-(j+1)}\alpha)+2\cos(2^{-j}\alpha))\widetilde{h}_j[4]\\
&+(4+4\cos(2^{-(j+1)}\alpha)+2\cos(2^{-j}\alpha))\widetilde{h}_j[5]+(1+4\cos(2^{-(j+1)}\alpha)\widetilde{h}_j[6]\\
&\quad=0,
\end{aligned} \tag{39}
$$

and for $k=2$,

$$\widetilde{h}[4] + (1 + 4\cos(2^{-(j+1)}\alpha)\widetilde{h}_j[5] + (4 + 4\cos(2^{-(j+1)}\alpha) + 2\cos(2^{-j}\alpha))\widetilde{h}_j[6] = 0. \tag{40}$$

Finally, we find $\widetilde{h}_j[3], \widetilde{h}_j[4], \widetilde{h}_j[5]$, and $\widetilde{h}_j[6]$ by the following formulas:

$$\begin{cases} \widetilde{h}_j[-1] = \widetilde{h}_j[6] = 0, \\ \widetilde{h}_j[0] = \widetilde{h}_j[5] = \dfrac{2\sqrt{2}\cos(2^{-(j+1)}\alpha) + \sqrt{2}}{12\cos(2^{-(j+1)}\alpha) + 4\cos(3\,2^{-(j+1)}\alpha)}, \\ \widetilde{h}_j[1] = \widetilde{h}_j[4] = \dfrac{-6\sqrt{2}\cos(2^{-(j+1)}\alpha) - 4\sqrt{2}\cos(2^{-j}\alpha) - 5\sqrt{2}}{12\cos(2^{-(j+1)}\alpha) + 4\cos(3\,2^{-(j+1)}\alpha)}, \\ \widetilde{h}_j[2] = \widetilde{h}_j[3] \\ \qquad = \dfrac{5\sqrt{2}\cos(2^{-(j+1)}\alpha) + 2\sqrt{2}\cos(2^{-j}\alpha) + \sqrt{2}\cos(3\,2^{-(j+1)}\alpha) + 2\sqrt{2}}{6\cos(2^{-(j+1)}\alpha) + 2\cos(3\,2^{-(j+1)}\alpha)}. \end{cases}$$

3.5 Sixth order cardinal Chebyshev B-splines

Let $\lambda = (\delta_1, \delta_2)$, where $\delta_1 = (\lambda_1, \lambda_2, \lambda_3) = (0, 0, 0)$, $\delta_2 = (\lambda_4, \lambda_5, \lambda_6) = (0, -i\alpha, i\alpha)$, and

$$N_\lambda^6(x) = N_{\delta_1}^3 * N_{\delta_2}^3(x).$$

Then, we assume that

$$\varphi_j(t) = N_{2^{-j}\lambda}^6(t). \tag{41}$$

Therefore,

$$\begin{aligned} \widehat{\varphi_j}(\omega) &= \widehat{N_{2^{-j}\delta_1}^3}(\omega)\widehat{N_{2^{-j}\delta_2}^3}(\omega), \\ &= \frac{1}{64}\Big(1 + (2 + 4\cos(2^{-(j+1)}\alpha))e^{-i\frac{\omega}{2}} + (5 + 8\cos(2^{-(j+1)}\alpha) \\ &\quad + 2\cos(2^{-j}\alpha))e^{-i\omega} + (8 + 8\cos(2^{-(j+1)}\alpha) + 4\cos(2^{-j}\alpha))e^{-i\frac{3\omega}{2}} \\ &\quad + (5 + 8\cos(2^{-(j+1)}\alpha) + 2\cos(2^{-j}\alpha))e^{-2i\omega} \\ &\quad + (2 + 4\cos(2^{-(j+1)}\alpha))e^{-i\frac{5\omega}{2}} + e^{-3i\omega}\Big)\widehat{N_{2^{-j}\lambda}^6}\left(\frac{\omega}{2}\right) \\ &= \mathcal{H}_j\left(\frac{\omega}{2}\right)\widehat{\varphi_{j+1}}\left(\frac{\omega}{2}\right). \end{aligned}$$

Thus, the normalized coefficients are expressed as

$$\begin{cases} h_j[0] = h_j[6] = \dfrac{\sqrt{2}}{24 + 32\cos(2^{-(j+1)}\alpha) + 8\cos(2^{-j}\alpha)}, \\ h_j[1] = h_j[5] = \dfrac{2\sqrt{2}\left(1 + 2\cos(2^{-(j+1)}\alpha)\right)}{24 + 32\cos(2^{-(j+1)}\alpha) + 8\cos(2^{-j}\alpha)}, \\ h_j[2] = h_j[4] = \dfrac{\sqrt{2}\left(5 + 8\cos(2^{-(j+1)}\alpha) + 2\cos(2^{-j}\alpha)\right)}{24 + 32\cos(2^{-(j+1)}\alpha) + 8\cos(2^{-j}\alpha)}, \\ h_j[3] = \dfrac{2\sqrt{2}\left(4 + 4\cos(2^{-(j+1)}\alpha) + 2\cos(2^{-j}\alpha)\right)}{24 + 32\cos(2^{-(j+1)}\alpha) + 8\cos(2^{-j}\alpha)}. \end{cases}$$

As in previous instances, let us assume that $\widetilde{h}_j[-1]$, $\widetilde{h}_j[0]$, $\widetilde{h}_j[1]$, $\widetilde{h}_j[2]$, $\widetilde{h}_j[3]$, $\widetilde{h}_j[4]$, $\widetilde{h}_j[5]$, $\widetilde{h}_j[6]$, and $\widetilde{h}_j[7]$, where

$$\widetilde{h}_j[-1] = \widetilde{h}_j[7], \quad \widetilde{h}_j[0] = \widetilde{h}_j[6], \quad \widetilde{h}_j[1] = \widetilde{h}_j[5], \quad \widetilde{h}_j[2] = \widetilde{h}_j[4].$$

The relation (14) implies

$$\widetilde{h}_j[3] + 2\widetilde{h}_j[4] + 2\widetilde{h}_j[5] + 2\widetilde{h}_j[6] + 2\widetilde{h}_j[7] = \sqrt{2}. \tag{42}$$

Using (10), we find, for $k = 0$

$$\begin{aligned} &\left(4 + 4\cos(2^{-(j+1)}\alpha) + 2\cos(2^{-j}\alpha)\right)\widetilde{h}_j[3] + \left(5 + 8\cos(2^{-(j+1)}\alpha) + 2\cos(2^{-j}\alpha)\right)\widetilde{h}_j[4] \\ &\quad + \left(2 + 4\cos(2^{-(j+1)}\alpha)\right)\widetilde{h}_j[5] + \widetilde{h}_j[6] = \frac{24 + 32\cos(2^{-(j+1)}\alpha) + 8\cos(2^{-j}\alpha)}{2\sqrt{2}}, \end{aligned} \tag{43}$$

for $k = 1$,

$$\begin{aligned} &\left(2 + 4\cos(2^{-(j+1)}\alpha)\right)\widetilde{h}_j[3] + \left(6 + 8\cos(2^{-(j+1)}\alpha) + 2\cos(2^{-j}\alpha)\right)\widetilde{h}_j[4] \\ &+ \left(8 + 8\cos(2^{-(j+1)}\alpha) + 4\cos(2^{-j}\alpha)\right)\widetilde{h}_j[5] \\ &+ \left(5 + 8\cos(2^{-(j+1)}\alpha) + 2\cos(2^{-j}\alpha)\right)\widetilde{h}_j[6] \\ &+ \left(2 + 4\cos(2^{-(j+1)}\alpha)\right)\widetilde{h}_j[7] = 0, \end{aligned} \tag{44}$$

for $k = 2$,

$$\begin{aligned} &\widetilde{h}_j[4] + \left(2 + 4\cos(2^{-(j+1)}\alpha)\right)\widetilde{h}_j[5] \\ &+ \left(5 + 8\cos(2^{-(j+1)}\alpha) + 2\cos(2^{-j}\alpha)\right)\widetilde{h}_j[6] \end{aligned}$$

$$+\left(8+8\cos(2^{-(j+1)}\alpha)+4\cos(2^{-j}\alpha)\right)\widetilde{h}_j[7]=0, \tag{45}$$

and for $k=3$,

$$\widetilde{h}_j[6]+\left(2+4\cos(2^{-(j+1)}\alpha)\right)\widetilde{h}_j[7]=0. \tag{46}$$

We take the following additional condition to simplify the computation:

$$\sum_{k=-6}^{2}(-1)^k\widetilde{h}_j[1-k]=0.$$

Finally, we can derive explicit formulas of $\widetilde{h}_j[3], \widetilde{h}_j[4], \widetilde{h}_j[5], \widetilde{h}_j[6]$, and $\widetilde{h}_j[7]$ as follows:

$$\begin{cases}
\widetilde{h}_j[-1]=\widetilde{h}_j[7]=\dfrac{-8\sqrt{2}\beta^2-9\sqrt{2}\beta-\sqrt{2}\beta\beta_2-2\sqrt{2}}{64\beta^2+48\beta+16\beta\beta_2^2+64\beta^2\beta_2+64\beta\beta_2},\\
\widetilde{h}_j[0]=\widetilde{h}_j[6]=\dfrac{16\sqrt{2}\beta^3+26\sqrt{2}\beta^2+13\sqrt{2}\beta+2\sqrt{2}\beta^2\beta_2+\sqrt{2}\beta\beta_2+2\sqrt{2}}{32\beta^2+24\beta+8\beta\beta_2^2+32\beta^2\beta_2+32\beta\beta_2},\\
\widetilde{h}_j[1]=\widetilde{h}_j[5]=\dfrac{-8\sqrt{2}\beta-\sqrt{2}\beta_2-5\sqrt{2}}{8\beta_2+8},\\
\widetilde{h}_j[2]=\widetilde{h}_j[4]\\
\qquad=\dfrac{-16\sqrt{2}\beta^3-18\sqrt{2}\beta^2-7\sqrt{2}\beta+2\sqrt{2}\beta\beta_2^2+6\sqrt{2}\beta^2\beta_2+7\sqrt{2}\beta\beta_2-2\sqrt{2}}{32\beta^2+24\beta+8\beta\beta_2^2+32\beta^2\beta_2+32\beta\beta_2},\\
\widetilde{h}_j[3]=\dfrac{64\sqrt{2}\beta^3+112\sqrt{2}\beta^2+51\sqrt{2}\beta+6\sqrt{2}\beta\beta_2^2+40\sqrt{2}\beta^2\beta_2+33\sqrt{2}\beta\beta_2+2\sqrt{2}}{32\beta^2+24\beta+8\beta\beta_2^2+32\beta^2\beta_2+32\beta\beta_2},
\end{cases}$$

where

$$\beta=\cos\left(2^{-(j+1)}\alpha\right),\quad \beta_2=\cos\left(2^{-j}\alpha\right).$$

The figures presented below (Figure 1) illustrate the scaling and wavelet functions associated with the previously obtained biorthogonal filter banks.

4 Application of nonstationary biorthogonal filter banks for image compression

In this section of our comparative study, we analyze the performance of nonstationary biorthogonal filter banks, derived in the previous section with parameters $\mathbf{n}=\mathbf{6}$, in comparison to the widely used Daubechies biorthogonal

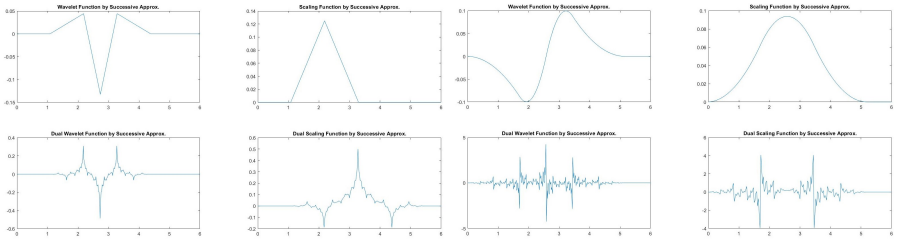

(a) φ_j, $\widetilde{\varphi}_j$, ψ_j, and $\widetilde{\varphi}_j$ for $\alpha = 0$, $j = 0$, and $n = 2$

(b) φ_j, $\widetilde{\varphi}_j$, ψ_j and $\widetilde{\varphi}_j$ for $\alpha = 0$, $j = 0$ and $n = 3$

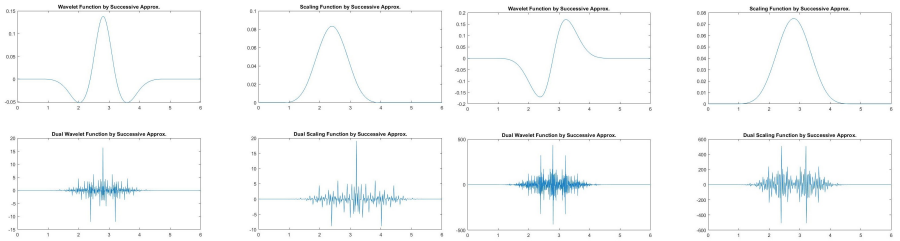

(c) φ_j, $\widetilde{\varphi}_j$, ψ_j, and $\widetilde{\varphi}_j$ for $\alpha = 0$, $j = 0$, and $n = 4$

(d) φ_j, $\widetilde{\varphi}_j$, ψ_j, and $\widetilde{\varphi}_j$ for $\alpha = 0$, $j = 0$, and $n = 5$

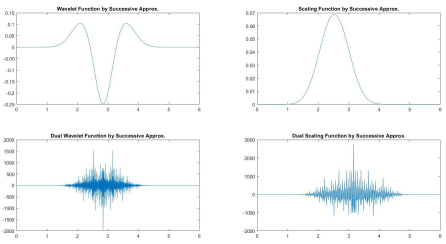

(e) φ_j, $\widetilde{\varphi}_j$, ψ_j, and $\widetilde{\varphi}_j$ for $\alpha = 0$, $j = 0$, and $n = 6$

Figure 1: Curves of scaling functions and wavelet functions

filter bior **bior 3.3**, **bior 4.4**, and **bior 5.5** [3]. The evaluation is conducted using the peak signal-to-noise ratio (PSNR) quality measure. The images considered in our study include pepper, bamboo, Barbara, lighthouse, boat, X-ray, and a textured image. The results of our analysis are presented in Table 1:

Table 1: Comparison of PSNR values for different images using stationary and nonstationary biorthogonal filter banks **(PS-NS)**.

Filter / Image	**bior 3.3**	**bior 4.4**	**bior 5.5**	**PS-NS**	**Optimal value of α**
Pepper image	373.0289	321.8209	317.6718	377.4309	**0.4**
Bamboo image	373.3974	312.1773	310.2757	376.0176	**1.4**
Barbara image	370.5101	312.7138	311.3224	373.5105	**1.4**
Lighthouse image	368.791	315.1341	312.1767	372.6814	**3**
Boat image	369.5577	316.4587	312.8915	372.7301	**0.1**
X-ray image	374.7837	321.2239	317.7600	379.4312	**0.4**
Textured image	372.4533	309.4582	305.5483	375.9778	**1.3**

Nonstationary filters optimized with an adaptive parameter α consistently offer better image reconstruction quality, as measured by a higher PSNR. Although the improvement varies depending on the image, this demonstrates the potential of nonstationary filters to outperform traditional biorthogonal approaches in terms of reconstruction fidelity.

In this section, we further analyze the effectiveness of these filter banks in image compression. Beyond the PSNR measure discussed earlier, we evaluate compression performance by quantifying the number of zeros introduced in the processed image. A higher count of zeros signifies greater compression efficiency, as it indicates a substantial reduction in redundant information

while retaining key image details. This metric is crucial for minimizing file size while maintaining satisfactory visual quality.

For each image, the parameter α is optimized to maximize the number of zeros, ensuring the best compression performance for the specific image. Thresholds are selected adaptively based on the characteristics of each image, striking a balance between maintaining visual quality and enhancing compression efficiency.

Table 2: Comparison of the number of zeros in the image after compression using stationary and nonstationary biorthogonal filter banks **(PS-NS)**.

Image	**Filter** / **Threshold**	**bior 3.3**	**bior 4.4**	**bior 5.5**	**PS-NS**	**Optimal value of α**
Pepper image	0.01	200271	195713	197236	202269	**3.4**
	0.05	201226	202617	204126	203773	**5.5**
	0.1	201408	202871	204126	205864	**5.6**
	0.15	201698	203119	204618	207672	**5.6**
	0.2	202298	203660	205135	207453	**5.4**
Bamboo image	0.1	205408	203566	203099	203737	**0.1**
	0.2	217290	217299	218389	218952	**0.1**
	0.3	223279	223417	224895	226805	**7.9**
	0.4	227922	228209	229755	232402	**7.9**
	0.5	232562	233066	234571	236767	**7.9**
Barbara image	0.1	193788	193613	194121	195190	**0.1**
	0.2	199199	199351	200434	203116	**0.2**
	0.3	203980	203945	204867	208590	**7.8**
	0.4	209261	209146	210240	214263	**7.9**
	0.5	213573	213464	214480	218510	**7.9**
Lighthouse image	0.1	200554	200951	201971	202509	**0.2**
	0.15	201904	202386	203638	204443	**2.3**
	0.2	202665	203358	204573	205806	**2.5**
	0.25	203531	204284	205498	206993	**3**
	0.3	204524	205309	206534	208083	**3**

Boat image	0.15	202593	203857	205311	206093	**5.3**
	0.3	206465	207617	208973	210035	**7.4**
	0.45	209932	210944	212315	213802	**7.3**
	0.6	212121	213224	214562	217194	**7.3**
	0.75	214717	215921	217330	220750	**7.2**
X-ray image	0.05	201017	202083	203617	203654	**4.6**
	0.1	201263	202711	204266	206469	**4.8**
	0.15	201330	202797	204349	209284	**4.8**
	0.2	232677	234175	235987	238573	**4.5**
	0.25	238801	240088	241793	244086	**7.4**
Textured image	0.05	202284	197225	197596	206985	**0.1**
	0.1	211203	208244	207600	212592	**0.1**
	0.15	216815	215130	214592	217219	**0.1**
	0.2	221580	220335	219984	221975	**0.1**
	0.25	225770	225134	225145	226346	**0.1**

The nonstationary filter consistently outperforms all other filters, achieving the highest number of zeros across all threshold values and images. This performance is particularly notable when compared to **bior 5.5**, highlighting its superior effectiveness in compression (Table 2).

The figures presented below (Figure 2–8) provide a qualitative evaluation of the reconstructed images after compression using the nonstationary biorthogonal filter bank **PS-NS**. These visualizations validate the filter's capability to achieve high compression efficiency without compromising perceptual image quality.

(a) Original pepper image. (b) Reconstructed pepper im-(c) Reconstructed pepper image for $th = 0.01$ and $\alpha = 3.4$.age for $th = 0.2$ and $\alpha = 5$.

Figure 2: Visualization of the original pepper image and its reconstructions with nonstationary filter.

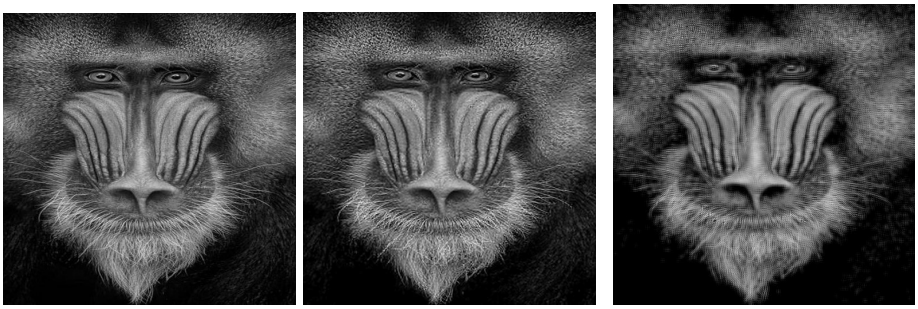

(a) Original mandrill image. (b) Reconstructed mandrill image for $th = 0.1$ and $\alpha = 0.1$.(c) Reconstructed mandrill image for $th = 0.5$ and $\alpha = 7.9$.

Figure 3: Visualization of the original mandrill image and its reconstructions with nonstationary filter.

(a) Original Barbara image. (b) Reconstructed Barbara image for $th = 0.1$ and $\alpha = 0.1$. (c) Reconstructed Barbara image for $th = 0.5$ and $\alpha = 7.9$.

Figure 4: Visualization of the original Barbara image and its reconstructions with nonstationary filter.

(a) Original lighthouse image. (b) Reconstructed lighthouse image for $th = 0.1$ and $\alpha = 0.2$.(c) Reconstructed lighthouse image for $th = 0.3$ and $\alpha = 3$.

Figure 5: Visualization of the original lighthouse image and its reconstructions with nonstationary filter.

(a) Original boat image. (b) Reconstructed boat image for $th = 0.15$ and $\alpha = 5.3$. (c) Reconstructed boat image for $th = 0.75$ and $\alpha = 7.2$.

Figure 6: Visualization of the original boat image and its reconstructions with nonstationary filter.

(a) Original X-ray image. (b) Reconstructed X-ray image for $th = 0.2$ and $\alpha = 4.5$. (c) Reconstructed X-ray image for $th = 0.25$ and $\alpha = 7.4$.

Figure 7: Visualization of the original X-ray image and its reconstructions with nonstationary filter.

(a) Original textured image. (b) Reconstructed textured image for $th = 0.2$ and $\alpha = 0.1$. (c) Reconstructed textured image for $th = 0.25$ and $\alpha = 0.1$.

Figure 8: Visualization of the original textured image and its reconstructions with nonstationary filter.

5 Conclusion

In conclusion, nonstationary biorthogonal wavelets are powerful tools for signal analysis, with recent advancements showcasing the utility of cardinal Chebyshev B-splines in their construction. The proposed method simplifies filter design by explicitly formulating filters and dual filters at all scaling levels, enabling efficient implementation through numerical methods like Gauss elimination or LU factorization. This streamlined approach, combined with the practical applications of nonstationary wavelets, underscores their importance in image processing.

Filters based on cardinal Chebyshev B-splines offer potential improvements in compression quality and computational efficiency, although performance may depend on the specific characteristics of the images processed.

Future research could focus on optimizing the method for high-dimensional data and integrating it into machine learning workflows, broadening the applicability of nonstationary wavelets across scientific and engineering domains.

Acknowledgements

The authors sincerely appreciate the constructive feedback and valuable suggestions provided by the anonymous referees and the editor.

References

[1] Boor, C., DeVore, R.A. and Ron, A. *On the construction of multivariate (pre) wavelets,* Constr. Approx. 9 (1993) 123–166.

[2] Brahimi, M., Melkemi, K. and Boussaad, A. *Design of nonstationary wavelets through the positive solution of Bezout's equation,* J. Interdiscip. Math. 24(3), (2021) 553–565.

[3] Daubechies, I. Ten lectures on wavelets, SIAM. 1992.

[4] Gasquet, C. and Witomski, P. *Analyse de Fourier et applications: filtrage, calcul numérique, ondelettes,* Elsevier Masson, 1990.

[5] Lee, Y.J. and Yoon, J. *Analysis of compactly supported nonstationary biorthogonal wavelet systems based on exponential B-splines,*In Abstract and Applied Analysis, vol. 2011, no. 1, p. 593436. Hindawi Publishing Corporation, 2011.

[6] Mallat, S.G. *Multiresolution approximations and wavelet orthonormal bases of* $L^2(\mathbb{R})$, Trans. Am. Math. Soc. 315(1) (1989) 69–87.

[7] Mazure, M.L., and Melkemi, K. Orthonormality of Cardinal Chebyshev B-spline Bases in Weighted Sobolev Spaces, Constr. Approx. 18(3) (2002) 387–415.

[8] Melkemi, K. *Orthogonalité des B-splines de Chebyshev cardinales dans un espace de Sobolev pondéré,* PhD diss., University Joseph-Fourier-Grenoble I, 1999.

[9] Soman, K. P. Insight into wavelets: from theory to practice, PHI Learning Pvt. Ltd, 2010.

[10] Vonesch, C., Blu, T., and Unser, M. Generalized Daubechies wavelet families, IEEE Trans. Signal Process. 55(9) (2007) 4415-4429.

[11] Zhang, B., Zheng, H., Zhou, J., and Pan, L. Construction of a family of non-stationary biorthogonal wavelets, J. Inequ. Appl. 1 (2019) 1–15.